

CrossMark  
click for updates

Cite this: DOI: 10.1039/c6nj01080f

# Functional liquid crystalline gels through multi-scale hierarchical self-assembly of LAPONITE<sup>®</sup> and amidodiol<sup>†</sup>

Rohini Kuttipavil Narayanan, Neethu Kalloor Sadanandhan, Renjith Sasi and Sudha Janardhanan Devaki\*

Herein we demonstrate the design and synthesis of liquid crystalline gels through multi-scale hierarchical self-assembly of LAPONITE<sup>®</sup> and amidodiol in water. These two components interact with each other through non-covalent interactions, such as hydrogen bonding and ion–dipole interactions, to form highly ordered superstructures in different dimensions and length scales. Effects of concentration of amidodiol and timescale on specific modes of packing were studied using various microscopic and spectroscopic techniques, such as PLM, SEM, TEM, XRD, rheology and FTIR. Presence of hydroxyl groups was confirmed by chemical analysis. A plausible mechanism for the formation of superstructures in functionalized LAPONITE<sup>®</sup>–amidodiol gel (FLAG) was proposed. Electrochemical impedance studies of the FLAG showed low charge transfer resistance (245 Ω) with a stable rectangular electrochemical window (–0.4 V to 1.5 V). Galvanostatic studies revealed good cycling stability with a specific capacitance of 1856 mF g<sup>–1</sup>. Results suggest that FLAGs can be exploited as an efficient gel electrolyte in energy storage devices.

Received (in Montpellier, France)  
8th April 2016,  
Accepted 19th August 2016

DOI: 10.1039/c6nj01080f

www.rsc.org/njc

## 1 Introduction

Hybrid liquid crystalline materials with self-assembled superstructures and specific modes of packing along with desired functionalities are reported for potential applications in drug delivery, sensors, display devices, energy storage, *etc.*<sup>1–5</sup> Development of liquid crystalline functional gels through self-organization of organic–inorganic molecular systems has recently become a significant area of research because of the synergistic properties arising from the molecular level self-assembly of inorganic–organic hybrid materials.<sup>6,7</sup> The supramolecular self-assembly approach through non-covalent interactions, such as hydrogen bonding, van der Waals' interactions, ionic bonding, charge-transfer and electrostatic interactions has thriving significance for the design of functional hybrid liquid crystalline gels.<sup>8,9</sup> The design of liquid crystalline functional materials using tailor made molecular gelators containing amide and hydroxyl linkages offers new features.<sup>10,11</sup> Inter and intramolecular hydrogen bonds between amide linkages are reported to be responsible for the functional properties in proteins and in many synthetic polyamides.<sup>12–15</sup> The liquid crystalline formation of polyester–amide prepared from amidodiol (AMD) was reported earlier from our group.<sup>16,17</sup>

Amidodiol possesses diamide and dihydroxyl groups and is expected to form self-organized macroscopic structures through extensive intermolecular hydrogen bond interactions. Liquid crystalline properties exhibited by polyester amide are attributed to the intermolecular hydrogen bond interactions between amide–amide and amide–ester groups. Studies on hybrid soft materials formed by the self-organization of low molecular weight organic molecules and inorganic layered materials, such as LAPONITE<sup>®</sup>, are gaining importance in many biochemical applications.<sup>18,19</sup>

LAPONITE<sup>®</sup> is a synthetic hectorite clay having layered hydrous sodium magnesium silicate, and possesses a high degree of structural regularity. LAPONITE<sup>®</sup> is made up of discoid platelets of magnesium lithium silicate (Si<sub>8</sub>[Mg<sub>5.5</sub>Li<sub>0.4</sub>O<sub>24.0</sub>]H<sub>4</sub>O<sub>24</sub>Na<sub>0.7</sub>) with a thickness of approximately 1 nm, and diameter of approximately 30 nm (Fig. S1, ESI<sup>†</sup>).<sup>20,21</sup> LAPONITE<sup>®</sup> discs are endowed with structural features such as hydroxyl groups, Lewis and Brønsted acidity, exchangeable interlayer cations, and nano-dimensions of the individual layers. The silanol groups located at the edges of the LAPONITE<sup>®</sup> sheets can be modified with organic compounds, such as thiol, amine, or long hydrocarbon chains.<sup>22,23</sup> Ruzicka and Gabriel *et al.* extensively studied LAPONITE<sup>®</sup>–water interaction and the lyotropic liquid crystalline phases of LAPONITE<sup>®</sup> gels.<sup>24–26</sup> LAPONITE<sup>®</sup> clay particles have an asymmetric charge distribution as there is a net negative charge on the surface and a partial positive charge on the edges. Hence, they will not interact with all the neighbours, but they can lock together

Chemical Sciences and Technology Division, CSIR – National Institute for Interdisciplinary Science and Technology, Thiruvananthapuram, 695019, India.  
E-mail: Sudhagd2001@yahoo.co.in

<sup>†</sup> Electronic supplementary information (ESI) available. See DOI: 10.1039/c6nj01080f

in lower densities. LAPONITE<sup>®</sup> gel is stable for a long time, and no aging problem is observed. Such a low-density gel can act as a gel electrolyte and could be employed in energy storage devices. It was reported that the high aspect ratio of LAPONITE<sup>®</sup> clay platelets favors a superior transport property. It was reported that sodium ions present in LAPONITE<sup>®</sup> clay can be exchanged with lithium ions, and the conductivity can be increased to a large extent, and they also find application in energy storage devices.<sup>27,28</sup>

An electrolyte material must possess excellent ionic conductivity, mechanical stability, electrochemical and thermal stability and not suffer leakage of electrolyte.<sup>29</sup> The present liquid electrolyte systems possess good ionic conductivity, but have a fundamental limitation for long-term operation due to their evaporation and leakage.<sup>30,31</sup> In this respect, solid electrolytes possess special features like compactness, portability, reliability and lack of leakage, apart from superior mechanical properties and long-term stability, but have limitations such as low ionic conductivity and slow rates of diffusion. Gel electrolytes combine the merit of liquid electrolytes (high ionic conductivity) and solid electrolytes (good mechanical stability, lack of leakage, compactness, portability). They are considered to be superior candidates as electrolytes due to their three-dimensional gel network, which facilitates ion transportation.<sup>32,33</sup> Compared with organogels, hydrogels provide an environmentally friendly green approach and low cost route for the preparation of electrolyte materials.<sup>34</sup> The infiltration ability of polymer gel electrolyte is less favorable and hence the development of a water-based, environmentally friendly, highly reliable supramolecular hydrogel electrolyte that resists solvent leakage, and provides good mass transport is of importance. The self-assembled liquid crystalline materials forming well defined anisotropic conductive pathways can be considered as attractive alternatives for the electrolyte material. Liquid crystalline materials exhibit both temperature- or solution-induced 1D, 2D and 3D ordered mesophases with typical textures such as columnar, smectic and bicontinuous cubic phases with anisotropic channels capable of forming conductive pathways for the transport of charges and ions.<sup>35–38</sup> Liquid crystalline hydrogels are considered as better candidate electrolytes for energy storage systems because of their special features, such as compactness, portability, reliability, lack of leakage and a green approach in addition to well defined anisotropic pathways for charge conduction. Organic and polymer gel electrolytes were reported to be used in dye sensitized solar cells and lithium ion batteries.<sup>39–41</sup> LAPONITE<sup>®</sup> based gel electrolyte is a new area of research and may be a prospective alternative for organic based gel electrolytes. Thus, by combining the advantages of LAPONITE<sup>®</sup> and amidodiol, the development of hybrid liquid crystalline supramolecular hydrogels with self-assembled anisotropic structures can be considered as alternatives for gel electrolytes in energy storage devices.

The present work demonstrates the design of liquid crystalline functional gel prepared through non-covalent interactions of LAPONITE<sup>®</sup> and amidodiol by a multi-scale hierarchical self-assembly approach. Effects of time and concentration parameters of amidodiol in the design of liquid crystalline functional gels were studied. They were characterized using microscopic

techniques, such as PLM, SEM and TEM, rheology, XRD and FTIR spectroscopy. Finally, cyclic voltammetric and galvanostatic charge–discharge studies were carried out, which demonstrated it's application as electrolyte in energy storage devices.

## 2 Experimental

### 2.1 Reagents

LAPONITE<sup>®</sup> RD (Southern Clay Products) was used as received. It has a cation exchange capacity of 60 meq. per 100 g.  $\gamma$ -Butyrolactone (Fluka, Germany), hexamethylene diamine, isopropanol, acetone and methanol (SD Fine Chemicals Ltd, Bombay, India), potassium ferricyanide, potassium ferrocyanide, potassium chloride (Merck, India) were used without further purification. All the experiments were carried out using Milli-Q purified water.

### 2.2 Preparation of 1,6-bis(hydroxybutyramido)hexane

1,6-Bis(hydroxybutyramido)hexane (amidodiol, AMD) was prepared by the aminolysis of  $\gamma$ -butyrolactone using 1,6-hexamethylene diamine as per the earlier reported procedure. The white crystalline solid formed, was filtered and washed several times with isopropanol, then dried in vacuum and further recrystallized from 150 mL of 1:1 methanol–acetone mixture (yield: 95%, M.P.: 118.5 °C). The scheme for this is given in Fig. S2 (ESI<sup>†</sup>). Formation of AMD was confirmed by <sup>1</sup>H-NMR and <sup>13</sup>C-NMR, given in Fig. S3 (ESI<sup>†</sup>).

### 2.3 Preparation of functionalized LAPONITE<sup>®</sup>-amidodiol gel (FLAG)

0.05 g of LAPONITE<sup>®</sup> was dissolved in 1 mL of hot distilled water and then it was thoroughly mixed with 1 mL of 1% amidodiol in water at 60 °C for 5 minutes. Then, the sample was kept undisturbed at room temperature for 24 hours and a transparent soft gel was obtained. FLAGs were prepared by varying the percentage of AMD (0.4% to 1.0%) and are designated as FLAG1, FLAG2, FLAG3, and FLAG4, respectively. A control sample was prepared using the same procedure but in the absence of AMD, and designated as LAP. Experimental details for the preparation of the FLAGs are shown in Table S1 (ESI<sup>†</sup>).

### 2.4 Electrochemical studies

ITO plates were cut into of 2 × 2 cm pieces using a glass cutter and were subjected to 5 minutes of cleaning in acetone, isopropanol, and distilled water by ultrasonication and were dried. The test cells, fabricated by sandwiching FLAG4 hydrogel between transparent conducting ITO-coated glass electrodes, were used for cyclic voltammetric (CV) and galvanostatic charge–discharge (GCD) studies. The specific capacitance values were calculated from the following equation using GCD results

$$\text{Specific capacitance} = (I\Delta t)/(m\Delta v)$$

where,  $I$  is the discharge current in amperes,  $\Delta t$  is the discharging time,  $\Delta v$  is the potential window during the discharge process, and  $m$  is the mass of the electrode materials in grams.

## 2.5 Characterizations

FTIR spectroscopic measurements were made with a fully computerized Nicolet Impact 400D FTIR spectrophotometer. Materials were mixed thoroughly with potassium bromide and compressed into pellets before recording. All spectra were corrected for the presence of moisture and carbon dioxide in the optical path. Wide angle X-ray scattering (WAXS) measurements were performed using a XEUSS SAXS/WAXS system by Xenocs. Cu K $\alpha$ , with wavelength  $\lambda \sim 1.54 \text{ \AA}$ , was used as the source. For SEM measurements, samples were subjected to thin gold coating using a JEOL JFC-1200 fine coater. The probing side was inserted into a JEOL JSM-5600 LV scanning electron microscope for taking photographs. TEM measurements were carried out using an FEI TECNAI G2 30 S-TWIN with an accelerating voltage of 100 kV. For TEM measurements, the samples were drop casted on a formvar coated copper grid and dried in vacuum at room temperature. Liquid crystalline phase formation was observed under a polarized light microscope (PLM) (Olympus BX51 equipped with a camera). The rheological properties of the sample were measured using a modular Compact Rheometer (MCR150, Anton Paar) with cone-and-plate geometry (CP 50-1/Ti  $d = 49.98 \text{ mm}$ , concentricity  $8 \text{ \mu m}$  and parallelity  $5 \text{ \mu m}$ , angle =  $0.991$ , truncation  $51 \text{ \mu m}$ ) and a solvent trap was utilized to minimize evaporation at a set measurement temperature of  $25 \text{ }^\circ\text{C}$ . Each mixture first underwent an oscillatory strain sweep ( $\gamma = 0.005\text{--}100\%$ ) at a constant frequency of  $1 \text{ Hz}$  and then conducted frequency sweep measurement at  $1\%$  oscillatory amplitude strain. Subsequently, dynamic or steady shear experiments were performed with the shear rate ranging from  $0.01$  to  $100 \text{ s}^{-1}$ . Electrochemical studies were carried out with CHI6211B electrochemical analyzer. GCE was modified with LAP and FLAG4 by drop casting gel on the electrode, then followed by air drying and were designated as LAP/GCE and FLAG/GCE, respectively. All the potentials were recorded using Ag/AgCl as the reference electrode and platinum wire as the counter electrode. The electrochemical impedance measurements were performed in a frequency range from  $0.1 \text{ Hz}$  to  $10 \text{ kHz}$  at an open circuit potential of  $1 \text{ V}$  in a three-electrode, one-compartment electrochemical cell. The electrochemical impedance measurements were performed with potassium ferrocyanide/ferricyanide solution for GCE, LAP/GCE and FLAG/GCE. Prior to electrochemical experiments, GCE was polished with  $0.03 \text{ micron}$  alumina and ultrasonically cleaned for about  $5 \text{ minutes}$  in doubly distilled water. Cyclic voltammetric and galvanostatic studies were carried out using a VSP potentiostat/galvanostat (Biologic Instruments) by fabricating test cells using ITO electrodes. All the experiments were carried out at  $25 \text{ }^\circ\text{C} \pm 5 \text{ }^\circ\text{C}$ . Before performing the experiments, the solution was purged with nitrogen gas for  $10 \text{ minutes}$ . Ionic conductivity was measured with a JENWAY 3540 pH and conductivity meter.

## 3 Results and discussion

### 3.1 Evolution of supramolecular self-assembly

The effect of composition of the components, such as LAPONITE<sup>®</sup> and amidodiol, on the evolution of the morphology was

studied using various microscopic techniques such as PLM, SEM and TEM. The observed results were further complemented with the results generated from XRD, rheology and FTIR. FLAGs of varying compositions were prepared by mixing aqueous solutions of LAPONITE<sup>®</sup> and AMD at room temperature. Studies showed that gelation time and gel strength of FLAGs depended on the concentration of the components and time. It has been observed that dilute aqueous LAPONITE<sup>®</sup> solutions ( $<2 \text{ wt}\%$ ) initially appeared as a sol and later changed into a transparent gel. However, when the LAPONITE<sup>®</sup> concentration is increased to  $>5 \text{ wt}\%$ , it immediately transforms into an opaque gel. Observation of LAPONITE<sup>®</sup> gels (LAP) under PLM showed the formation of nematic texture and is depicted in Fig. S4 (ESI<sup>†</sup>). Our observation is strengthened by the studies reported by Ruzicka and Gabriel *et al.*<sup>24,25</sup> Liquid crystalline phase formation is favored by the ordered arrangement of the discs in a particular direction and gelation is attributed due to the three dimensional network formations of discs (Fig. S5, ESI<sup>†</sup>). The SEM image of LAPONITE<sup>®</sup> sol before functionalization exhibited isolated disc-like morphology and is provided in Fig. S6 (ESI<sup>†</sup>).

The PLM image of AMD is given in Fig. S7a (ESI<sup>†</sup>), which shows the formation of birefringent sheets. The SEM image of AMD also confirmed the sheet-like morphology, as shown in Fig. S7b (ESI<sup>†</sup>). The SEM and PLM studies confirmed that AMD possess the potential for self-assembly with LAPONITE<sup>®</sup>. Effects of AMD on the gelation time, gel strength and formation of liquid crystalline phase formation were studied. It has been observed that there is an increase in the gel strength in presence of AMD. This may be due to the network formation established by the combined effect of various non-covalent interactions among the partial charges, Mg–OH and Si–OH groups present on the surface and edges of the LAPONITE<sup>®</sup> discs with diamide and dihydroxyl groups contributed by AMD.

Evolution of morphological changes in FLAGs were studied using various microscopic techniques such as PLM, SEM and TEM. FLAGs exhibited different mesophases depending upon the amount of amidodiol, LAPONITE<sup>®</sup> and time. The PLM image of the initial stage of FLAG1 is observed as birefringent distorted spherulites dispersed in an isotropic medium. This might be due to the random dispersion of functionalized LAPONITE<sup>®</sup> discs in the aqueous phase (Fig. 1a). The self-assembly of spherulites in FLAG1 is shown in Fig. 1b. Later, this entity was observed to be elongated by edge-to-edge interaction of functionalized LAPONITE<sup>®</sup> discs and the branched structures formed in FLAG2 are shown in Fig. 1c. Here, the self-assembled bilayer of AMD co-structures with the LAPONITE<sup>®</sup> discs in various ways. The branched quill and feather morphology of FLAG3 is shown in Fig. 1d and e. With increasing amount of AMD, varieties of branched nematic tapes were observed in FLAG4 and are shown in Fig. 1f. Further morphology of the FLAGs was studied by SEM and the images are shown in Fig. 2a–d. Fig. 2a shows the SEM image of a single disc with flowery edges of self-assembled AMD in FLAG1. The SEM image of freshly prepared FLAG2 exhibited thick edged isolated discs and later, these discs piled up hierarchically by edge-to-edge etching, as shown in Fig. 2b. This observation was supported by PLM studies. As the amount

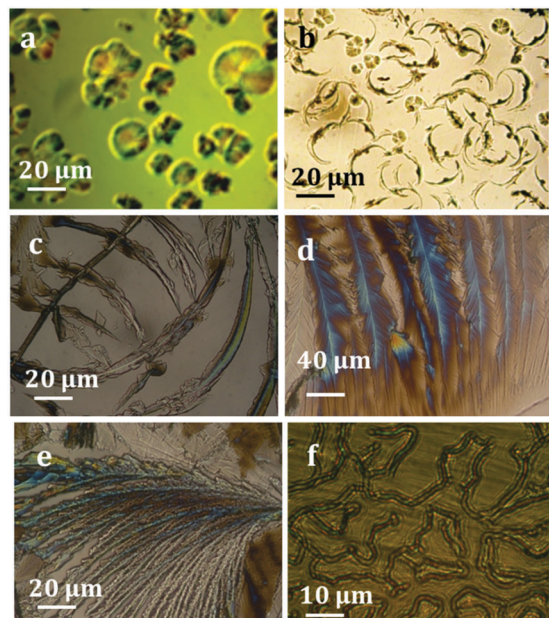


Fig. 1 PLM images of (a) spherulites in the initial stage of FLAG1, (b) self-assembling and co-structuring of FLAG1, (c) FLAG2, (d) and (e) feather and quill like morphology of FLAG3 and (f) branched tape like morphology of FLAG4.

of AMD increased, these domains transformed into feathers/plumes and tape like morphologies in FLAG3 and FLAG4, respectively, as shown in Fig. 2c and d, respectively. Thus, by controlling the experimental conditions, multi-scale hierarchical arrangement of the domains can be obtained for various liquid crystalline phases.

The TEM pictures of FLAG4 taken under different magnifications are shown in Fig. 3a and b. Micrographs exhibited tape like morphology and a number of well-defined dark fringes were observed inside the tape. The contrast in the TEM image strongly depends on their orientation with respect to the electron beam. Diffraction contrast is strong when the LAPONITE<sup>®</sup> nanodiscs

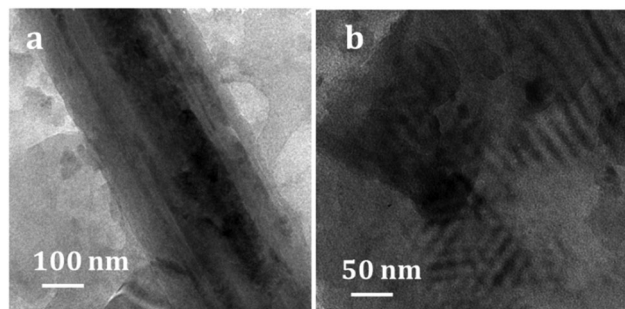


Fig. 3 (a) TEM image of FLAG4 showing tape morphology, (b) magnified image of tape like morphology in FLAG4 showing the Fresnel fringes of LAPONITE<sup>®</sup> discs.

are seen with their basal plane parallel to the electron beam. Pronounced Fresnel fringes appeared on each side of the diffracting platelets and are shown in Fig. 3b. These fringes are considered to originate from the development of various interactions among the individual moieties present in FLAG4.

The non-covalent interactions between LAPONITE<sup>®</sup> and AMD during the self-assembly process leading to the formation of supramolecular structures in FLAG4 were evidenced from the results obtained by various experimental studies, such as FTIR spectroscopy and XRD. The FTIR spectra of LAP, AMD and FLAG4 are shown in Fig. 4. The spectrum of LAP exhibited a band at 3640 cm<sup>-1</sup> attributed to the presence of Si-OH and Mg-OH stretching vibrations which are distinct to the varying micro environments in the LAPONITE<sup>®</sup> structure. It exhibited bands at 1640 cm<sup>-1</sup> (physisorbed water), 1007 cm<sup>-1</sup> (stretching vibration of Si-O and Si-O-Si moieties), and 640 cm<sup>-1</sup> (stretching vibration of Mg-O linkage). The FTIR spectrum of AMD exhibited characteristic amide I and amide II bands at 1636 cm<sup>-1</sup> (C=O stretching) and 1545 cm<sup>-1</sup> (C-N stretching in combination with N-H bending). The band at 3300 cm<sup>-1</sup> is attributed to -OH and -NH stretching vibrations of the AMD and the band at 2920 cm<sup>-1</sup> corresponds to the stretching vibrations of the -CH<sub>2</sub> moiety. The characteristic spectral bands of Mg-O (1007 cm<sup>-1</sup>) and

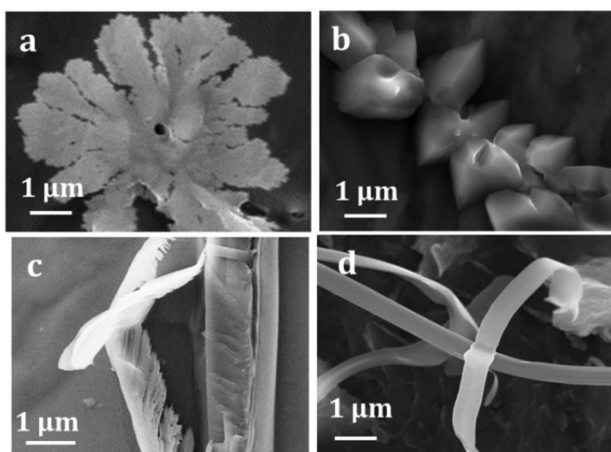


Fig. 2 SEM images of (a) freshly prepared FLAG1 in the initial stage, (b) FLAG2, (c) branched morphology of FLAG3, (d) the fibrillar tape like morphology of FLAG4.

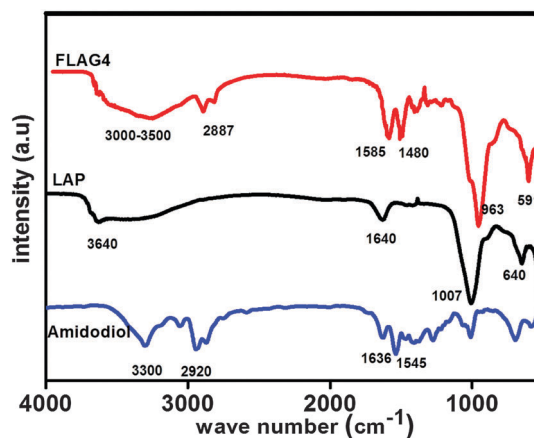


Fig. 4 FTIR spectra of LAP, AMD and FLAG4 showing the non-covalent interactions among LAPONITE<sup>®</sup>-LAPONITE<sup>®</sup>, LAPONITE<sup>®</sup>-amidodiol and amidodiol-amidodiol.

Si–O–Si ( $640\text{ cm}^{-1}$ ) observed in LAP are shifted to  $963\text{ cm}^{-1}$  and  $591\text{ cm}^{-1}$ , respectively, and the distinctive vibrations corresponding to amide bands present in AMD, observed at  $1636$  and  $1545\text{ cm}^{-1}$ , are measured to be shifted to  $1585\text{ cm}^{-1}$  and  $1480\text{ cm}^{-1}$  in FLAG4. Further, the characteristic bands of –OH and –NH stretching vibrations in LAP and AMD, appearing as a broad band at  $3000\text{--}3500\text{ cm}^{-1}$  in FLAG4, confirmed the extensive hydrogen bonding interaction between the LAPONITE<sup>®</sup> and AMD. The shifts in the characteristic bands of LAPONITE<sup>®</sup> and LAP revealed extensive hydrogen bonding and the non-covalent interactions between these two moieties induce the formation of self-assembled aggregates of mesophase and stable gel phase. Functional hydroxyl groups in FLAGS were estimated by chemical analysis. The hydroxyl value of LAP is  $0.94\text{ mmol g}^{-1}$ , which is increased to  $3.04\text{ mmol g}^{-1}$  in the case of FLAG4 confirming the enhancement of the functional groups. Thus, FLAGS are endowed with functional groups of amide and hydroxyl groups, apart from the unreacted charges, which can be exploited for many applications.

The  $d$ -spacing between the LAPONITE<sup>®</sup> discs and the dimension of the aggregates in FLAG was studied by XRD. The XRD spectra of AMD, LAPONITE<sup>®</sup> and FLAGS are shown in Fig. 5. The diffraction pattern of LAPONITE<sup>®</sup> exhibited a broad diffraction peak at  $2\theta = 6.64^\circ$  corresponding to inter planar  $d$ -spacing of  $\sim 13.3\text{ \AA}$  which can be related to the  $d_{001}$  basal plane oriented parallel to the substrate surface. The exact position of this peak may vary as a function of relative humidity. XRD of AMD exhibited well-defined sharp intense peaks at  $2\theta = 10^\circ, 15^\circ, 21^\circ, 23^\circ, 26^\circ, 30^\circ$  and  $32^\circ$  revealing its highly crystalline nature. Nevertheless, the XRD spectrum of FLAGS exhibited entirely different XRD patterns in terms of the shape and position of peaks in comparison to LAPONITE<sup>®</sup> and AMD, suggesting the formation of supramolecular structures. FLAGS exhibited two

peaks at lower angles between  $2\theta \sim 2^\circ$  to  $6^\circ$  revealing the formation of highly ordered supramolecular ensembles with the dimensions of  $30\text{--}40\text{ \AA}$  and a shift in the  $d$ -spacing of the LAPONITE<sup>®</sup> disc. The nature and position of this peak varied with the amount of amidodiol. In FLAG1, the peak at  $2\theta \sim 6.3^\circ$  ( $14.01\text{ \AA}$  corresponds to the shift in LAPONITE<sup>®</sup>  $d$ -spacing) and the peak at  $2\theta \sim 2.6^\circ$  ( $33.93\text{ \AA}$ ) agreed with the dimension of the ensemble whereas FLAG2 showed a broad peak at  $2\theta \sim 5.3^\circ$  ( $16.65\text{ \AA}$  shift in the  $d$ -spacing of LAPONITE<sup>®</sup>) and a sharp peak observed at  $2\theta \sim 2.4^\circ$  ( $36.76\text{ \AA}$ , related to the dimension of the supramolecular ensemble). FLAG3 showed a broad peak at  $2\theta \sim 5.2^\circ$  ( $16.97\text{ \AA}$ ) and a sharp peak observed at  $2\theta \sim 2.4^\circ$  ( $35.84\text{ \AA}$ , related to the dimension of the supramolecular ensemble). FLAG4 exhibited the peak at  $2\theta = 4.4^\circ$  ( $20.05\text{ \AA}$ ) and the peak at  $2\theta \sim 2.2^\circ$  ( $40.10\text{ \AA}$ ) agreeing with the dimension of the ensembles. The peaks corresponding to AMD is diminished in the FLAGS. The formation of these supramolecular ensembles was further supported by themorphological analysis by PLM and SEM.

The small angle XRD peaks confirm the formation of self-assembled supramolecular ensembles. The SAXS of FLAG1 is provided in the inset of Fig. 5. The  $d$ -values calculated are  $14.6\text{ \AA}$  and  $32.3\text{ \AA}$ . These values matched with the  $d$ -values calculated from WXR measurement [in FLAG1, the peak  $2\theta = 6.3^\circ$  ( $14.01\text{ \AA}$  corresponds to the shift in LAPONITE<sup>®</sup>  $d$ -spacing) and the peak at  $2\theta = \sim 2.6^\circ$  ( $33.93\text{ \AA}$ )].

The viscoelastic properties of composites depend on the size, shape, entanglement and periodicity of the components. Viscoelastic properties of gels are functions of critical oscillatory strain, phase angle, storage modulus, loss modulus and viscosity.<sup>42,43</sup> Dynamic amplitude strain sweep experiments at constant stress controlled conditions were conducted to observe the linear viscoelastic region in FLAGS, where the applied strain does not considerably affect the three-dimensional network structures. The linear regime is identified by plotting the stress-strain curve given in Fig. S8 (ESI<sup>†</sup>). The linear regime is observed for very low strain values  $\sim 1$  to  $2\%$  and is clearly visible in the plot. The storage modulus/loss modulus *versus* amplitude strain sweep profile of FLAGS is shown in Fig. S9 (ESI<sup>†</sup>). The crossover point indicates when the elastic nature of the gel is changed into its viscous nature. The crossover points obtained for FLAG1, FLAG2, FLAG3 and FLAG4 of  $3.5\%$ ,  $4.2\%$ ,  $5.6\%$ , and  $6.9\%$ , respectively, confirmed the role of AMD for establishing robust nature for FLAGS. Angular frequency dependent storage modulus and loss modulus of FLAGS and LAP were studied at constant strain ( $1\%$ ). Typical diagrams showing angular frequency *versus* storage modulus ( $G'$ ) and loss modulus ( $G''$ ) are shown in Fig. 6a. At the lower frequency region, the variation of  $G'$  and  $G''$  is independent of angular frequency where the applied frequency does not considerably affect the three-dimensional structure of the gels which is a signature of true gel formation. The gap between storage and loss modulus increases with increase in concentration of AMD, and reveals that, as the amount of AMD increases, the elastic modulus is enhanced due to the high extent of cross-linking density. The difference in the modulus for LAP, FLAG1, FLAG2, FLAG3 and FLAG4 are observed to be  $730\text{ Pa}$ ,  $938\text{ Pa}$ ,  $984\text{ Pa}$ ,  $1073\text{ Pa}$ , and  $1290\text{ Pa}$ , respectively. Time-dependent

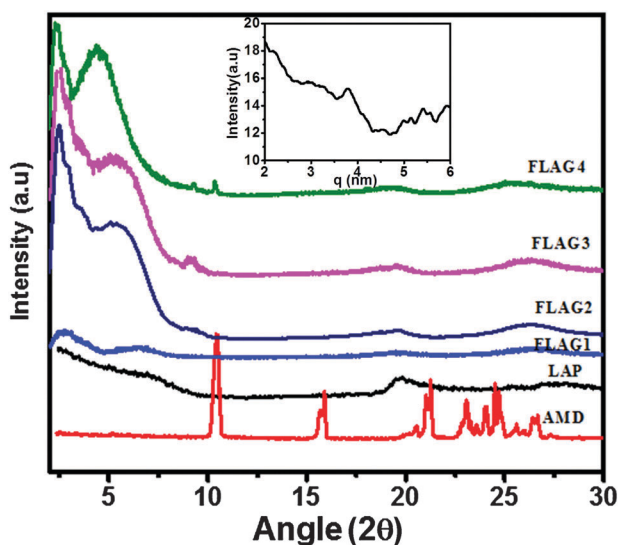


Fig. 5 XRD of AMD, LAPONITE<sup>®</sup>, FLAG1, FLAG2, FLAG3 and FLAG4 showing the self-assembled aggregates of LAPONITE<sup>®</sup> and AMD while retaining the crystalline ordering of LAPONITE<sup>®</sup> in FLAGS. Inset showing the SAXS of FLAG1 confirms the formation of self-assembled aggregates.

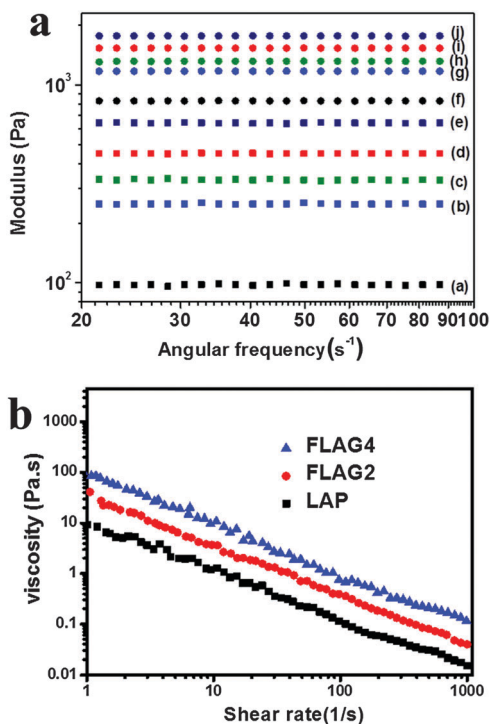


Fig. 6 (a) Double logarithmic plot of angular frequency *versus* loss and storage modulus profile for LAP and FLAGs. (a) LAP  $G''$ , (b) FLAG1  $G''$ , (c) FLAG2  $G''$ , (d) FLAG3  $G''$ , (e) FLAG4  $G''$ , (f) LAP  $G'$ , (g) FLAG1  $G'$ , (h) FLAG2  $G'$ , (i) FLAG3  $G'$ , (j) FLAG4  $G'$ . (b) Double logarithmic plot of shear rate *versus* viscosity of FLAGs showing shear thinning behaviour.

rheological studies were carried out to study and predict the effect of aging on the gel strength. Freshly prepared gel samples showed storage moduli of 831.3, 1193.7, 1295.26, 1552.12, and 2085.3 Pa for LAP, FLAG1, FLAG2, FLAG3, and FLAG4, respectively. However, storage modulus values were found to increase with time, which attributed to the establishment of a greater density of hydrogen bond interactions between these two entities in various fashions. Time-dependent changes in the storage modulus of FLAG4 were measured as 2341, 2784, 3321, 3890, 4512, 4514, 4515 Pa, which is quite high elastic and solid like behaviour compared with the freshly prepared sample, and is shown in Fig. S10 (ESI<sup>†</sup>). After one week, the storage modulus was observed to make only very small variations. The time-dependent IR spectra provided in Fig. S11 (ESI<sup>†</sup>) confirm the increase in the density of hydrogen bonding with time.

It has been reported in Ericksen's theory that liquid crystalline materials may exhibit high degree of structural ordering and the domains can be arranged in a specific fashion to obtain molecular orientation. Under shear flow, structural rearrangement may occur in the internal polydomain structure of liquid crystalline materials. Each domain is having a high degree of molecular orientation. With increasing shear rate, there is a successive destruction of the polydomain structure into smaller domains. Accordingly, the lamellar liquid crystalline phases of FLAGs are composed of ordered hierarchical structures of polydomains. With increasing shear force, they slide upon one another to form smaller domains accompanied by a sudden decrease in the

viscosity value. The double logarithmic plot of shear rate *versus* viscosity is given in Fig. 6b. The viscosity decreases with increase in shear rate according to the power law behaviour,  $\eta = K\dot{\gamma}^n$ . The straight line obtained in Fig. 6b showed a fitting to the power law behaviour. This observation supports the shear thinning behaviour. This is supported by the observation made by Onogi and Asada in the rheological studies of liquid crystalline materials.<sup>44,45</sup>

### 3.2 Mechanism for the formation of mesophases

A plausible mechanism for the formation of various mesophases was manifested from the studies made by FTIR, microscopic analysis, XRD and rheology. Water molecules penetrate into the interlamellar space and push the LAPONITE<sup>®</sup> discs apart. At high concentrations, LAPONITE<sup>®</sup> suspension spontaneously turns into an opaque gel. At low concentrations, initially fluid like LAPONITE<sup>®</sup> turns into gel phase after 24 hours. The nematic liquid crystalline phase formation is due to the periodicity arising from the face-to-face mutual orientation among the functional LAPONITE<sup>®</sup> discs. Formation of various liquid crystalline phases in FLAGs can be explained due to changes in the periodicity, defect formation, molecular packing and nano-segregation during the mesophase formation, which varies with the experimental conditions. As we have reported above, FLAG comprises highly exfoliated nanodiscs with negative charges on the surface, partial positive charge on the edges and Mg-OH and Si-OH groups at the broken edges. AMD contains two amide groups and two hydroxyl groups. Hence, there is competition between various non-covalent interactions among LAPONITE<sup>®</sup>-LAPONITE<sup>®</sup>, LAPONITE<sup>®</sup>-AMD and AMD-AMD *via* hydrogen bonding, dipole-dipole and electrostatic interactions of hydroxyl groups, amide groups and ionic charges. Apart from this, LAPONITE<sup>®</sup>-AMD-water interactions also play a crucial role in the liquid crystalline phase formation. FLAGs are observed as transparent gels and a photograph of this is given in Fig. 7.

Initially, all FLAGs observed as sols and under PLM appeared isotropic due to the random dispersion of both AMD and LAPONITE<sup>®</sup>. Later, due to supramolecular interactions, AMD is non-covalently attached to the LAPONITE<sup>®</sup> edges and they form spherulites in the isotropic medium. Slowly these spherulites elongate by a growth process of etching and self-assembly. They self-assemble in two ways, either zig-zag to form a bush or edge-to-edge etching to form feather/plume type structures. Later, in the presence of excess AMD, more self-assembled AMD adheres on the surface of the branched stems (templates) to form arrays of highly birefringent feathers or leaves and multi-walled tapes by

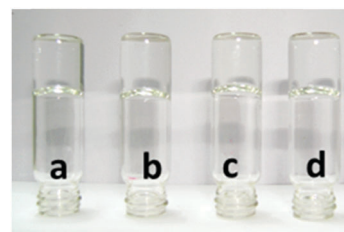
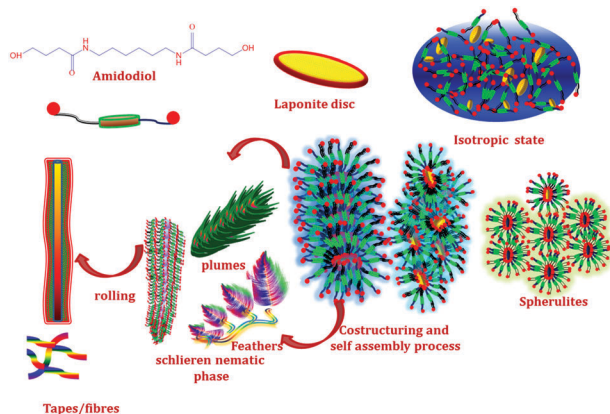


Fig. 7 Photograph of (a) FLAG1, (b) FLAG2, (c) FLAG3 and (d) FLAG4.



**Scheme 1** Schematic representation of the formation of various mesophases via supramolecular self-assembly of LAPONITE<sup>®</sup> and AMD.

co-structuring and self-assembly processes among functionalized LAPONITE<sup>®</sup>s and AMD. This observation is supported by our earlier studies made on polyaniline–clay nanocomposites.<sup>46</sup> The various phases formed by FLAGs are further supported by the work done by previous researchers.<sup>47</sup> They suggested that organo-modified LAPONITE<sup>®</sup>s can undergo various structural transformation such as star, vesicular and more disorganized bundle-like structures based on the experimental conditions.<sup>48,49</sup> Thus, by controlling the concentration and time parameters in FLAG, we can design mesophases through non-covalent interactions by a self-assembly approach. This type of synthetic design can be exploited for the development of multi-scale and hierarchical functional materials from low molecular weight molecules. A schematic showing various structural arrangements among the components in the FLAG are depicted in Scheme 1.

### 3.3 Electrochemical properties

Electrochemical properties were evaluated using various techniques such as cyclic voltammetry, electrochemical impedance spectroscopy and galvanostatic charge–discharge studies. The electrochemical impedance spectroscopy (EIS) is used to study the electron transfer properties of the surface modified electrodes. The EIS data were analyzed *via* Nyquist plot and it consists of two regions – a semicircle region lying in the  $Z'$  axis followed by a straight line. The semicircle region at higher range of frequencies corresponds to the electron transfer kinetics and the linear part at the lower range of frequencies represents diffusion limited electron transfer processes.<sup>50</sup> The Nyquist plots of GCE, LAP/GCE and FLAG/GCE with  $\text{Fe}(\text{CN})_6^{3-/4-}$  are shown in Fig. 8a. The equivalent circuit diagram used to fit the data is shown in the inset of Fig. 8a and is composed of solution resistance ( $R_s$ ), constant phase element (CPE,  $Q$ ), electron transfer resistance ( $R_{ct}$ ) and Warburg impedance ( $W$ ). With LAP/GCE, the diameter of the semicircle region decreases indicating a low electron transfer resistance. In the case of FLAG/GCE, the semicircle region again decreases and it exhibits very low impedance. The  $R_{ct}$  values of bare GCE, LAP/GCE and FLAG/GCE are 1124  $\Omega$ , 640  $\Omega$  and 245  $\Omega$ , respectively. The high conductivity of FLAG/GCE may be suggested due to high anisotropic liquid crystalline ordering of FLAG. The cyclic

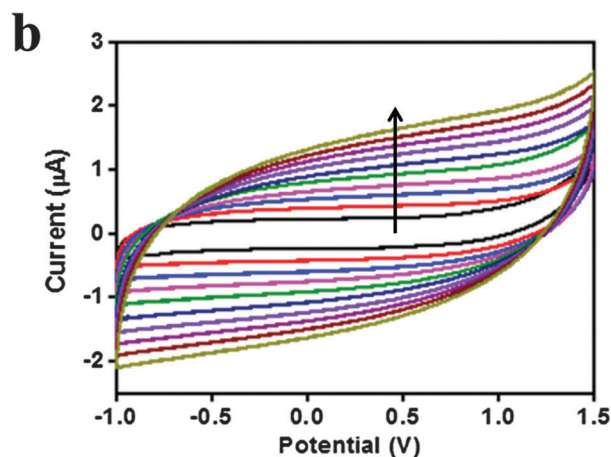
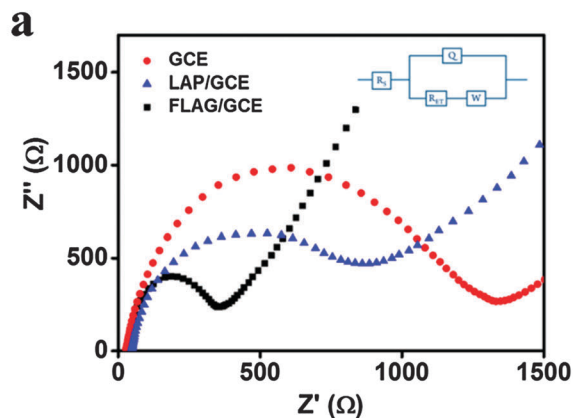


**Fig. 8** (a) Nyquist plots of GCE, LAP/GCE and FLAG/GCE. (b) Cyclic voltammograms of FLAG/GCE with scan rates ranging from 0.01 to 0.1  $\text{V s}^{-1}$ .

voltammograms of FLAG4 is shown in Fig. 8b. They showed a good rectangular electrochemical window between  $-1$  and  $1.5$  V and hence these gel electrolytes are suitable for application in capacitors and batteries. The stability of the electrochemical window is retained even at higher scan rates and with high current density.

The galvanostatic charge–discharge measurements were carried out within the potential window of 0 to 1.5 V at various current densities ranging from 0.02 to 0.41  $\text{A g}^{-1}$  and are shown in Fig. 9a. Galvanostatic charge–discharge studies showed symmetrical charge–discharge profiles suggesting that FLAG4 exhibits ideal electrical double layer capacitive behaviour without any redox reaction involved. For a constant current density of 0.02  $\text{A g}^{-1}$ , the specific capacitance of the cell was calculated as 1856  $\text{mF g}^{-1}$  illustrating the excellent energy storage capability of the material. The specific capacitances of FLAG4 were calculated to be 1856, 1799, 1676, 1640, 1610 and 1598  $\text{mF g}^{-1}$  at current densities of 0.02, 0.04, 0.06, 0.08, 0.16 and 0.41  $\text{mF g}^{-1}$ , respectively. On increasing the current density, we observed a steady lowering of specific capacitances due to faster discharging. Cycling performance plays an important role in determining the super capacitors for real applications.<sup>34,51</sup> Capacity retention of the device was analyzed by carrying out repetitive charging and discharging for 100 cycles. The variation of specific capacitance

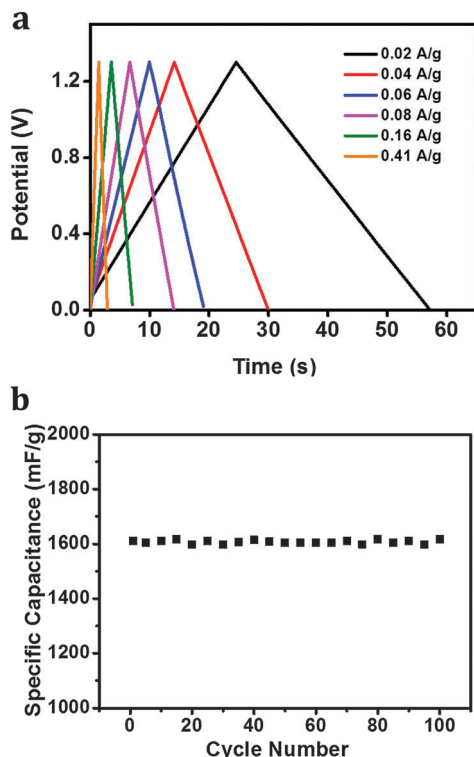


Fig. 9 (a) Charge–discharge voltage profiles at various current densities ranging from 0.005 to 0.2 A g<sup>-1</sup> (b) cycling stability of FLAG4 for 100 cycles: variation of specific capacitance with cycle number at a current density of 0.1 A g<sup>-1</sup>.

with cycle number is given in Fig. 9b. The device gave 99% retention of specific capacitance even after the 100th cycle indicating its high cycling stability. Cycling performance of FLAG4 for 100 cycles at a current density of 0.1 A g<sup>-1</sup> is shown in Fig. S12 (ESI<sup>†</sup>). The specific capacitance of FLAG4 is compared with the literature reports and is given in Table S2 (ESI<sup>†</sup>) which confirms better efficiency of FLAG4 as a gel electrolyte.<sup>52–54</sup>

FLAG exhibits an ionic conductivity value of 540 μS cm<sup>-1</sup>, attributed to the presence of Na<sup>+</sup> ions. The sodium ions which are present in the interlayer gallery dissociate and may be responsible for the ionic conductivity. The AMD moiety can induce an anisotropic liquid crystal ordering in the gel and lead to low impedance and ideal capacitive behaviour. It has been reported earlier that liquid crystalline ordering can enhance the conductivity by augmenting mobility of ions through the ordered channels which are present in between the domains.<sup>55,56</sup> The high conductivity and the viscoelastic properties of the FLAG, revealed its utility as prospective gel electrolyte for energy storage systems.

## 4 Conclusion

Morphological evolution studies through various techniques suggest that supramolecular self-assembly in FLAGs is a function of time and concentration of the components: LAPONITE<sup>®</sup>, amidodiols and water. Electrochemical results showed lower charge transfer resistance of 245 Ω with an excellent rectangular

electrochemical window of -1 to 1.5 V suggesting its utilization as a gel electrolyte for energy storage devices. Further galvanostatic charge–discharge studies using FLAG as an electrolyte in a super-capacitor showed a symmetrical charge–discharge profile, a specific capacitance of 1856 mF g<sup>-1</sup> for a constant current density of 0.02 A g<sup>-1</sup>, and very good cycling stability. These studies revealed that FLAG can be considered as an excellent electrolyte material in the area of energy storage.

## Acknowledgements

We are thankful to Dr A. Ajayaghosh, Director, CSIR-NIIST, Trivandrum, for the constant encouragement and support. We would also thank to Ms. Lucy Paul, Mr Kiran Mohan and Dr E. Bhoje Gowd for SEM, TEM and XRD analyses. We are also thankful for the financial support from CSIR network project MULTIFUN (CSC0101) and CSIR-SRF fellowship.

## Notes and references

- 1 K. Kanie and A. Muramatsu, *J. Am. Chem. Soc.*, 2005, **127**, 11578–11579.
- 2 A. Walcarius, *Chem. Mater.*, 2001, **13**, 3351–3372.
- 3 C. T. Nguyen and R. M. Kasi, *Chem. Commun.*, 2015, **51**, 12174–12177.
- 4 M. M. Qasim, A. A. Khan, A. Kostanyan, P. R. Kidambi, A. Cabrero-Vilatela, P. Braeuninger-Weimer, D. J. Gardiner, S. Hofmann and T. D. Wilkinson, *Nanoscale*, 2015, **7**, 14114–14120.
- 5 H. Song, N. Zhao, W. Qin, B. Duan, X. Ding, X. Wen, P. Qiu and X. Ba, *J. Mater. Chem. A*, 2015, **3**, 2128–2134.
- 6 G. Ungar, C. Tschierske, V. Abetz, R. Holyst, M. A. Bates, F. Liu, M. Prehm, R. Kieffer, X. Zeng, M. Walker, B. Glettner and A. Zywockinski, *Adv. Funct. Mater.*, 2011, **21**, 1296–1323.
- 7 T. Kato, N. Mizoshita and K. Kishimoto, *Angew. Chem., Int. Ed.*, 2006, **45**, 38–68.
- 8 C. M. Paleos and D. Tsiourvas, *Angew. Chem., Int. Ed. Engl.*, 1995, **34**, 1696–1711.
- 9 R. Daly, O. Kotova, M. Boese, T. Gunnlaugsson and J. J. Boland, *ACS Nano*, 2013, **7**, 4838–4845.
- 10 J. J. van Gorp, J. A. J. M. Vekemans and E. W. Meijer, *J. Am. Chem. Soc.*, 2002, **124**, 14759–14769.
- 11 K. Yabuuchi, E. Marfo-Owusu and T. Kato, *Org. Biomol. Chem.*, 2003, **1**, 3464–3469.
- 12 T. Kato and J. M. J. Frechet, *J. Am. Chem. Soc.*, 1989, **111**, 8533–8534.
- 13 H. Ringsdorf, R. Wüstefeld, E. Zerta, M. Ebert and J. H. Wendorff, *Angew. Chem., Int. Ed. Engl.*, 1989, **28**, 914–918.
- 14 K. Praefcke, D. Singer, B. Kohne, M. Ebert, A. Liebmann and J. H. Wendorff, *Liq. Cryst.*, 1991, **10**, 147–159.
- 15 K. Yamauchi, Y. Takashima, A. Hashidzume, H. Yamaguchi and A. Harada, *J. Am. Chem. Soc.*, 2008, **130**, 5024–5025.
- 16 J. D. Sudha, *J. Polym. Sci., Part A: Polym. Chem.*, 2000, **38**, 2469–2486.

- 17 J. D. Sudha and C. K. S. Pillai, *J. Polym. Sci., Part A: Polym. Chem.*, 2003, **41**, 335–346.
- 18 A. R. Hirst, I. A. Coates, T. R. Boucheteau, J. F. Miravet, B. Escuder, V. Castelletto, I. W. Hamley and D. K. Smith, *J. Am. Chem. Soc.*, 2008, **130**, 9113–9121.
- 19 L. Tao, Z. Huo, Y. Ding, L. Wang, J. Zhu, C. Zhang, X. Pan, M. K. Nazeeruddin, S. Dai and M. Gratzel, *J. Mater. Chem. A*, 2014, **2**, 15921–15930.
- 20 D. Bonn, H. Kellay, H. Tanaka, G. Wegdam and J. Meunier, *Langmuir*, 1999, **15**, 7534–7536.
- 21 N. Willenbacher, *J. Colloid Interface Sci.*, 1996, **182**, 501–510.
- 22 N. N. Herrera, J.-M. Letoffe, J.-P. Reymond and E. Bourgeat-Lami, *J. Mater. Chem.*, 2005, **15**, 863–871.
- 23 C. Teng, J. Qiao, J. Wang, L. Jiang and Y. Zhu, *ACS Nano*, 2016, **10**, 413–420.
- 24 B. Ruzicka, L. Zulian and G. Ruocco, *Phys. Rev. Lett.*, 2004, **93**, 258301.
- 25 J.-C. P. Gabriel, C. Sanchez and P. Davidson, *J. Phys. Chem.*, 1996, **100**, 11139–11143.
- 26 B. Ruzicka, E. Zaccarelli, L. Zulian, R. Angelini, M. Sztucki, A. Moussaïd, T. Narayanan and F. Sciortino, *Nat. Mater.*, 2011, **10**, 56–60.
- 27 J. L. Lutkenhaus, E. A. Olivetti, E. A. Verploegen, B. M. Cord, D. R. Sadoway and P. T. Hammond, *Langmuir*, 2007, **23**, 8515–8521.
- 28 M. Riley, P. S. Fedkiw and S. A. Khan, *J. Electrochem. Soc.*, 2002, **149**, A667–A674.
- 29 Z. Xue, D. He and X. Xie, *J. Mater. Chem. A*, 2015, **3**, 19218–19253.
- 30 J. M. Tarascon and M. Armand, *Nature*, 2001, **414**, 359–367.
- 31 J. B. Goodenough and Y. Kim, *Chem. Mater.*, 2010, **22**, 587–603.
- 32 A. Manuel Stephan, *Eur. Polym. J.*, 2006, **42**, 21–42.
- 33 Y. Wang and W.-H. Zhong, *ChemElectroChem*, 2015, **2**, 22–36.
- 34 N. A. Choudhury, S. Sampath and A. K. Shukla, *Energy Environ. Sci.*, 2009, **2**, 55–67.
- 35 M. Yoshio, T. Mukai, K. Kanie, M. Yoshizawa, H. Ohno and T. Kato, *Adv. Mater.*, 2002, **14**, 351–354.
- 36 D. Högberg, B. Soberats, S. Uchida, M. Yoshio, L. Kloo, H. Segawa and T. Kato, *Chem. Mater.*, 2014, **26**, 6496–6502.
- 37 X. Feng, L. Sosa-Vargas, S. Umadevi, T. Mori, Y. Shimizu and T. Hegmann, *Adv. Funct. Mater.*, 2015, **25**, 1180–1192.
- 38 J. Sakuda, E. Hosono, M. Yoshio, T. Ichikawa, T. Matsumoto, H. Ohno, H. Zhou and T. Kato, *Adv. Funct. Mater.*, 2015, **25**, 1206–1212.
- 39 Z. Huo, S. Dai, C. Zhang, F. Kong, X. Fang, L. Guo, W. Liu, L. Hu, X. Pan and K. Wang, *J. Phys. Chem. B*, 2008, **112**, 12927–12933.
- 40 K. Hanabusa, K. Hiratsuka, M. Kimura and H. Shirai, *Chem. Mater.*, 1999, **11**, 649–655.
- 41 I. Basumallick, P. Roy, A. Chatterjee, A. Bhattacharya, S. Chatterjee and S. Ghosh, *J. Power Sources*, 2006, **162**, 797–799.
- 42 J. Zhang, C. Daubert and E. A. Foegeding, *Rheol. Acta*, 2005, **44**, 622–630.
- 43 D. Xu, D. Bhatnagar, D. Gersappe, J. C. Sokolov, M. H. Rafailovich and J. Lombardi, *Macromolecules*, 2015, **48**, 840–846.
- 44 S. Onogi and T. Asada, in *Rheology*, ed. G. Astarita, G. Marrucci and L. Nicolais, Springer, US, 1980, ch. 9, pp. 127–147, DOI: 10.1007/978-1-4684-3740-9\_9.
- 45 G. G. Viola and D. G. Baird, *J. Rheol.*, 1986, **30**, 601–628.
- 46 J. D. Sudha, A. Pich, V. L. Reena, S. Sivakala and H.-J. P. Adler, *J. Mater. Chem.*, 2011, **21**, 16642–16650.
- 47 B. Dufour, P. Rannou, P. Fedorko, D. Djurado, J.-P. Travers and A. Pron, *Chem. Mater.*, 2001, **13**, 4032–4040.
- 48 A. Mouchid, E. Lécolier, H. Van Damme and P. Levitz, *Langmuir*, 1998, **14**, 4718–4723.
- 49 S. v. D. Jeroen, K. Susanne, L. Edward, P. Claire and M. R. Robert, *J. Phys.: Condens. Matter*, 2005, **17**, 2255.
- 50 E. Barsoukov and J. R. Macdonald, *Impedance Spectroscopy: Theory, Experiment, and Applications*, Wiley, 2005.
- 51 C. Masarapu, H. F. Zeng, K. H. Hung and B. Wei, *ACS Nano*, 2009, **3**, 2199–2206.
- 52 X. Peng, H. Liu, Q. Yin, J. Wu, P. Chen, G. Zhang, G. Liu, C. Wu and Y. Xie, *Nat. Commun.*, 2016, **7**, 11782.
- 53 P. Shaowu, D. Jue, G. Guozhen, Z. Ye, C. Peining, R. Jing and P. Huisheng, *J. Mater. Chem. A*, 2015, **3**, 6286–6290.
- 54 R. Singh and C. C. Tripathi, *Int. J. Electrochem. Sci.*, 2016, **11**, 6347–6355.
- 55 S. Cheng, D. M. Smith and C. Y. Li, *Macromolecules*, 2014, **47**, 3978–3986.
- 56 Y. Zhou, S.-k. Ahn, R. K. Lakhman, M. Gopinadhan, C. O. Osuji and R. M. Kasi, *Macromolecules*, 2011, **44**, 3924–3934.